DOI: 10.13009/EUCASS2022-4800
9TH EUROPEAN CONFERENCE FOR AERONAUTICS AND SPACE SCIENCES (EUCASS)

Verification of the Technology Combination Analysis Tool (TCAT) for space logistics modeling in the Earth-Moon system

*Sung Wook Paek**, *Philipp Huber***, *Flavio Brancato***, *Marc-André Chavy-Macdonald***, *Jean-Paul Kneib***, *Reda Cristofoletti**

**City, University of London*
Northampton Square, EC1V0HB London, United Kingdom
***École Polytechnique Fédérale de Lausanne*
EPFL Space Center (eSpace), 1015 Lausanne, Switzerland

Abstract

The Technology Combination Analysis Tool (TCAT) is a Python-based space transportation modelling package. with feasibility assessment applications in active debris removal (ADR), on-orbit servicing (OOS), and constellation deployment. This paper reports the preliminary results of (1) adding an electric propulsion (EP) model to TCAT and (2) cataloging a database of EP systems with flight heritage.

1. Introduction

The Technology Combination Analysis Tool (TCAT) is a space transportation modeler for prototyping and assessing the feasibility of various scenarios such as active debris removal (ADR), on-orbit servicing (OOS), and constellation deployment to name a few. Its precursor, written in Matlab, was used for the CNES-funded OTV-2 study by Swiss Space Center EPFL (Ref. [1]); the aim then was to find the most performant ADR mission architectures and technologies in low-Earth orbits (LEOs).

The earliest version of TCAT has then been adapted and improved to extend its applicability from the LEOs to the cislunar space ('cislunar' version for simplicity) [2]. It demonstrated the feasibility of spacecraft sizing/modeling with chemical propulsion in the Earth-Moon system. Written in python, the 2020 version's accuracy was verified with the Apollo 11 mission as a benchmark.

The scope of this paper is one of further variations/applications from the cislunar version. Some preliminary results of adopting electric propulsion (EP) are reported along with lessons learned. Also presented here is a separate but relevant project in which the specifications of space-flown EP systems were surveyed.

1.1 Background & Literature Review

There was an overarching need from eSpace and its clients to extend the capabilities of the earliest TCAT after the OTV-2 study. Amongst the potential extension options therefrom, it was decided to include mass calculation models by subsystems constituting a spacecraft. The rationale behind this decision was that mass calculation models can be validated readily compared to trajectories or launch windows calculation. Thus, the cislunar version (2020) included mass models whose assumptions and specifics are detailed in Ref. [2].

A comprehensive literature review was performed before embarking on this project to identify the gaps, trends and research/development needs [3]. As can be seen in Table 1, the sequence/topology of a campaign (a series of missions) is an input if the infrastructure size is an output, or vice versa, except for Bounova's Object Process Network tool [4]. Optimizing all of these aspects is a nontrivial task, especially if sub-optimization is required for EP. Due to the modeling complexity, EP trajectories are usually replaced by a simple spiral centered around the Sun (interplanetary) or Earth (LEOs) in literature.

DOI: 10.13009/EUCASS2022-4800

			General			Features																Implementation						
			Design Focus			Mission Options											Input (I) / Output (O) (opt.: *)			Measures of Effectiveness (opt.: *)			Software					Model	
			Logistics / Architecture	Trajectory	Spacecraft / Subsystems	Single Mission	Campaign	High-Thrust	Low-Thrust	Prepositioning	ISRU	Active Debris Removal	Aerocapture	Cargo/Crew Delivery	Constellations	On-Orbit Servicing	Infrastructure Sizing (e. g. S/C, Habitat)	Mission Sequence (Maneuver Order)	Network Route	Cost (Monetized)	Mass-Related (e. g. IMLEO)	Safety/Risk	Graphical User Interface	Standalone Executable	MATLAB Interface / Usage	MS Excel Interace / Usage	Python Interface / Usage	Flow Network (Graph Theory)	Object Process Network
Framework	Year	Author/Version				Interdependency		Propulsion		Resources		Type																	
-	2005	Bounova	✓		✓	✓	✓	✓	✓	✓	✓		✓	✓			O	O	O	✓	✓	✓			✓				✓
SpaceNet	2009	Grogan / v2.5r2	✓			✓	✓	✓		✓				✓			I	I	I		✓	✓	✓	✓		✓	✓		
GMCNF+	2013	Ishimatsu	✓			✓		✓			✓		✓	✓			I	O	O*		✓*				✓	✓		✓	
	2016	Ho	✓			✓	✓	✓		✓	✓		✓	✓			I	O	O*		✓*				✓	✓		✓	
	2020	Jagannatha	✓	✓		✓	✓	✓	✓	✓			✓	✓			I	O	O*		✓*				✓	✓		✓	
EXAMINE+	2008	Komar	✓		✓	✓	✓	✓	✓	✓	✓		✓	✓			O	I	I		✓*	✓				✓			
	2014	Arney	✓		✓	✓	✓	✓	✓	✓	✓			✓			O	I	I		✓							✓	
STK (Astrogator)	-	AGI		✓		✓	✓	✓	✓				✓	✓	✓		I(O)	I	I		✓		✓	✓	✓				
GMAT	-	NASA		✓		✓	✓	✓	✓				✓	✓	✓	✓	I(O)	I	I	?	?	?	✓	✓	✓		✓		
TCAT	-	eSpace			✓	✓		✓				✓		✓			O	I	I		✓						✓		

Table 1: Example Overview of the properties and capabilities of various space logistics tools.

After the literature review, two possible options for the extension of TCAT were considered: implementing (i) the model for calculating EP system mass and (ii) the model for cost/risk/safety analysis. The first option was chosen by the student carrying out this project for a thesis, whose choice was also more aligned with the prior extension to the cislunar version. Although EP has been becoming more popular in space logistics modeling, it seemed that novel contributions could be made not only in this project but also in its follow-ups such as uncertainties or cost estimation.

1.2 External software

An external software, called FreeFlyer (v7.6), was used to simulate EP trajectories and was integrated into the framework of TCAT (cislunar version). The FreeFlyer performs numerical integration to propagate the state of a spacecraft in time. To propagate a spacecraft during a finite burn maneuver, FreeFlyer integrates the mass flow equation (i.e. the specific impulse definition) alongside the following equations of motion:

$$\vec{F} = m(\vec{a}_{central\_body} + \vec{a}_{other\_bodies} + \vec{a}_{drag} + \vec{a}_{SRP} + \vec{a}_{thrust} + \vec{a}_{etc}) \quad \textbf{(1)}$$

where the acceleration terms represent the contributions from the Earth, other celestial bodies (e.g., the Moon), atmospheric drag, solar radiation pressure, spacecraft propulsion, and other forces. The gravitational forces of the Moon or the Sun were not included to simplify the optimizer design and ease its convergence process. A Runge-Kutta propagator, often used for finite maneuvers and interplanetary transfers, was used with the 8th order propagation and the 9th order error control. The use of FreeFlyer was preferred to GMAT in this project because detailed documentation and help services were available at no cost for student projects. However, the use of GMAT may still be considered for the follow-up projects because it is completely open-source and also python-interfaceable in its latest versions.

1.3 TCAT internals

The cislunar version of TCAT featured a control logic that varied the mass of spacecraft subsystems as well as the onboard propellant mass, followed by a convergence check within its mission. Using the flowchart and terms in Figure 1, for instance, applying a plan (a high-thrust maneuver) would incur the following steps: (i) calculate the Δv and the duration that are necessary to perform it, unless these values are already specified by the user as input; (ii) compute the

DOI: 10.13009/EUCASS2022-4800

propellant mass corresponding to the Δv; (iii) consume the propellant mass within the corresponding spacecraft. Depending on the user input, the initially guessed amount of propellant will then be too small or too large. In either case, a custom algorithm within TCAT can simply add or subtract an incremental propellant mass. To prevent the propellant mass from becoming too small or even negative, the following convergence criteria was used:

$$| m_{prop\_remaining} - C_{contingency} m_{prop\_inital} | < \Delta m \quad \textbf{(2)}$$

such that the remaining propellant mass would not deviate too much from the threshold (contingency) mass by more than the mass margin (Δm). Figure 1 contains several terms used in general mission design, and their definitions in the context of TCAT are provided below for further clarification. First, a "scenario" is a specific configuration of a use case that is described by a number of parameters. These parameters usually describe the details of the service architecture, the systems design, the orbits and the operations. The code base of a scenario is linked to the code base of a use case and thus separate from the core of TCAT as well. A fleet is a collection of satellites, launchers, ground segments and so forth that are used to fulfill a scenario. Fleet components that have a similar purpose or design can be grouped together within a fleet. The code base linked to the definition, management and use of a fleet is part of the core of TCAT and thus independent of a use case. Lastly, a plan is a chronologically ordered collection of phases, which are required to execute a scenario. It can more or less be thought of as the mission sequence. The code base linked to plans is part of the core of TCAT and independent of a use case.

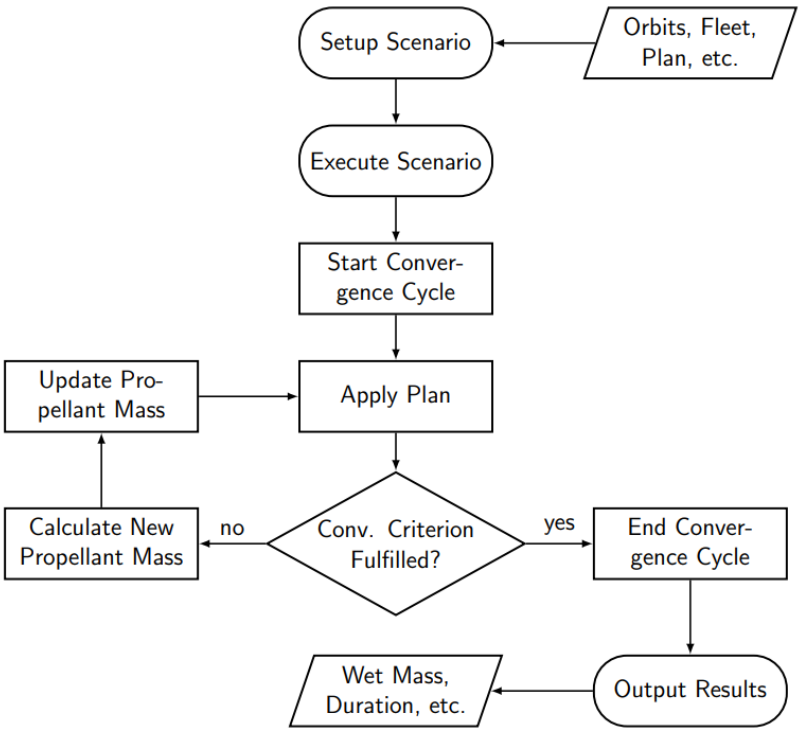

Figure 1. Illustration of the control flow in the previous version of TCAT (cislunar).

2. Methodology

The control flow in Figure 2 actually features two distinct convergence cycles, the first of which also varies the mass of the subsystems and checks for convergence within each mission. The second convergence cycle (which is illustrated and relevant to this project) is dedicated to only varying the propellant mass. The convergence algorithm introduced above was fine for the case of high-thrust propulsion, but could no longer be used for low-thrust propulsion. The problem basically arises through the coupling of the trajectory performance measures and the spacecraft mass; for low-thrust trajectories, however, calculating the Δv and the propellant mass can not be done separately, as the Δv that is necessary is dependent on the mass of the spacecraft.

DOI: 10.13009/EUCASS2022-4800

2.1 Control Flow

During the implementation of the low-thrust lunar transfers into TCAT, it became apparent that changes had to be made to the core of TCAT. Specifically, FreeFlyer terminates the simulation and returns an error if a spacecraft's propellant runs out before completing the simulation. Each time during the convergence cycle that the propellant mass was sufficient, a newly introduced value, referred to as the upper boundary, was set to the initial propellant mass of the iteration. If the propellant mass was insufficient, the newly introduced lower boundary was set to the initial propellant mass. Using this method, the new propellant mass for the successive iteration could always be calculated as the mean of the two boundaries and should have slowly converged towards the desired value (Figure 2).

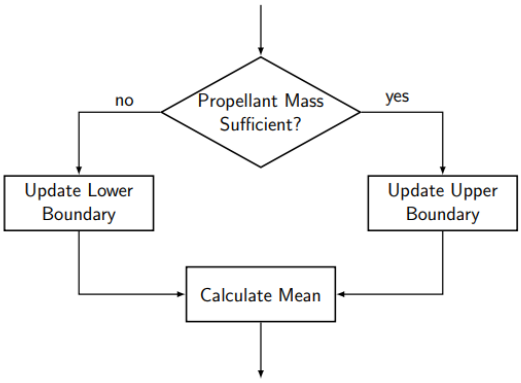

Figure 2. Algorithm to calculate the new propellant mass as the mean of an upper and a lower boundary.

Although this scheme seemed to work, several cases were observed where upper and lower boundaries were approaching and getting stuck at the same value which does not correspond to the convergence criteria. This tendency resulted in an ever-running loop. Therefore, a minor modification was made in the algorithm such that the initial guess for propellant mass is the maximum possible amount at first, i. e. the maximum tank capacity of the spacecraft, which is subtracted by a small amount during each successive iteration. This would cause the algorithm to be much slower in general but should prevent "missing" the desired amount of propellant and getting stuck in a loop again.

While the algorithm seemed to work fine in the beginning, a similar behavior as in the first case was found where the propellant mass was not able to converge. Only a Cowell integrator had been considered (not RK89) up to this point as well as the first case. The size of the margin (Δm) in the convergence criterion given in Equation (2) had to be increased, which would increase the deviation of the propellant mass from the desired contingency but also allow for a relatively robust behavior of the algorithm. It was at this time that the reason for this previously unstable convergence was found to be a discrepancy between the accuracy TCAT anticipates and the accuracy that is provided by FreeFlyer, when using the Cowell integrator.

Replacing the Cowell integrator with an RK89 integrator resolved all of the issues related to the mismatch between the converged value ($m_{prop\_remaining}$) and the contingency level ($C_{contingency}\, m_{prop\_initial}$) that had previously arisen when using the Cowell integrator. The troubleshooting process also revealed that simply updating the scheme of the upper boundary and the lower boundary makes the propellant mass converge to zero while our goal was to make it converge to the specified contingency mass. As a consequence, slight changes to the way the boundary values were calculated had to be made for the final version of the algorithm. Now, the upper boundary would initially be set to the maximum tank capacity and each time the propellant mass was sufficient, but not fulfilling the convergence criterion yet, a certain value was subtracted from the upper boundary. This value was given by

$$m_{sub} = \left| 2(m_{prop\_remaining} - C_{contingeny} m_{prop\_inital}) \right| \quad \textbf{(3)}$$

which equals the twice the left-hand side of Equation (2). The number two in Equation (3) will cancel out during the binary search step through which the mean of the two boundary values are taken by multiplying ½. In the final algorithm depicted in Figure 3, everything that is drawn in gray has already been present in the previous control flow in Figure 1, whereas everything drawn in black is new to indicate additions or modifications. For example, FreeFlyer directly returns the propellant mass that was used for the transfer, omitting the need to calculate it from the Δv in the first place.

DOI: 10.13009/EUCASS2022-4800

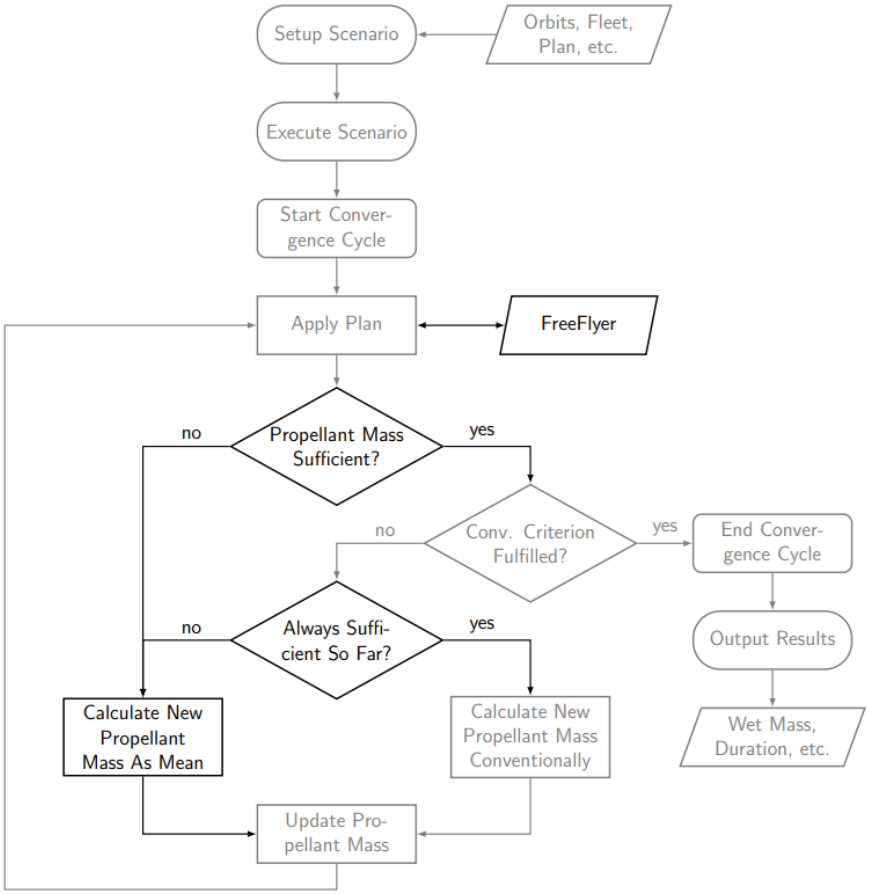

Figure 3: Illustration of the control flow in the extended version of TCAT.

2.2 EP trajectories

Unlike high-thrust transfers, where there exist a few general strategies that can be implemented quickly (e.g., Hohmann transfer), general strategies do not really exist for the case of low-thrust. Different missions will make use of very different low-thrust trajectories. A modeling approach for low-thrust Earth-Moon trajectories similar to Colombo et al. (2007) that considered a variety of low-thrust lunar trajectories for the European Student Moon Orbiter (ESMO) mission [5]. Each trajectory consists of three phases: a spiraling-up phase around the Earth, a lunar capture phase and a spiraling-down phase around the Moon. These three phases are designed independently and then linked together, after which they are optimized with a local optimizer for low-thrust trajectories. They assume a continuous tangential thrust profile, as this provides the fastest way for a spacecraft to spiral up or down. The only exception to continuous thrusting is when the spacecraft enters the umbra of the Earth or the Moon. Starting from an initial geostationary transfer orbit (GTO) around Earth, the spacecraft trajectory is propagated until it reaches an apogee of 280 000 kilometers. Next, the lunar capture orbit is found with an aposelene of 60 000 kilometers via backward calculation (10-day simulation time) from the final Moon orbit. It should be noted that due to their approach of backward propagating the spacecraft, the mass of the spacecraft in the final Moon orbit had to be estimated before starting the propagation. For the modeling of such trajectories within TCAT, it was decided against this backward propagation approach. After reaching the apogee at 330 000 kilometers, lunar capture is assumed and the location of the spacecraft is “manually moved” to a circular orbit around the Moon in a radius of 60 000 kilometers. Figure 4 illustrates top-down views of spiraling-up and spiraling down trajectories from Earth and to the Moon, respectively, implemented in FreeFlyer. Figure 5 shows the time history of the spacecraft’s position and its remaining propellant mass.

DOI: 10.13009/EUCASS2022-4800

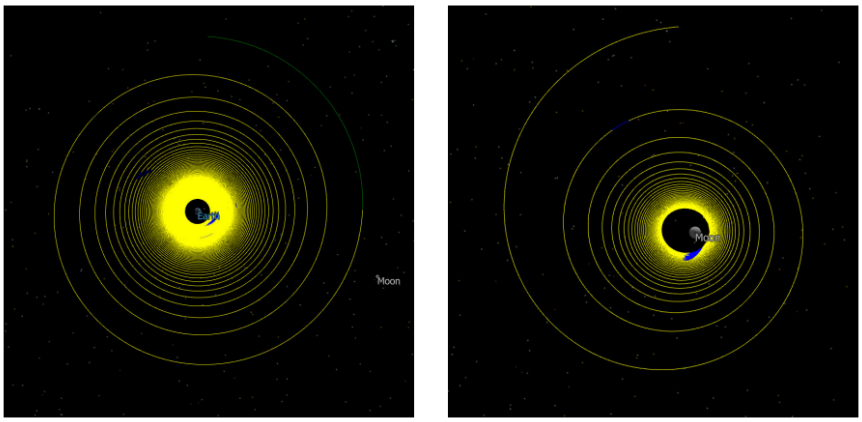

Figure 4: Earth spiraling-up phase (left) and Moon spiraling-down phase (right), visualized in FreeFlyer.

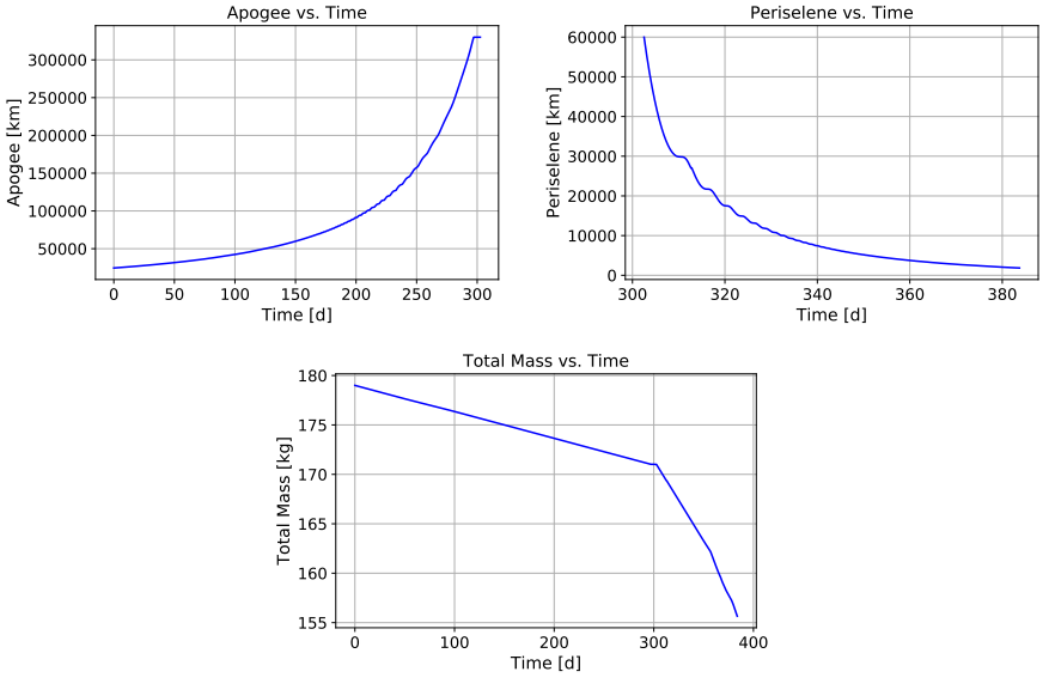

Figure 5: Apogee (upper left), periselene (upper right) and total mass (bottom) against time for low-thrust lunar trajectory modeled in TCAT.

3. Discussion

In addition to ESMO, one more mission was considered for benchmarking - SMART-1 which is the first of the Small Missions for Advanced Research in Technology. The SMART-1 mission was ESA's first lunar mission and successfully demonstrated the use of advanced ion propulsion for navigation and several mission control techniques. Unlike ESMO which was not launched, SMART-1 spacecraft actually flew the lunar orbit from 2003 to 2006.

3.1 Case studies

The ESMO mission considered chemical propulsion (CP) in the end, so its dry mass could not be directly translated into EP, meaning that the EP-dry-mass of the ESMO contains uncertainties that cannot be quantified (136.7 kg in Table 2). The second mission for benchmarking was the SMART-1 mission that successfully demonstrated the use of advanced ion propulsion in 2003. The total dry mass of the SMART-1 could be matched by allocating assumed subsystem masses in TCAT, unlike the wet mass of the ESMO.

DOI: 10.13009/EUCASS2022-4800

Table 2: 'Actual' values of the two benchmarked missions

	ESMO (EP equivalent)	**SMART-1**
Wet mass [kg]	180	367
Dry mass [kg]	136.7	287
Propellant mass (used) [kg]	25.3	80
Thrust [N]	0.02	0.068
Specific impulse [s]	3250	1640

The two example missions were tested in the extended TCAT to see whether its spacecraft sizing/optimizing algorithm yielded similar values in propellanr mass. Table 2 summarizes the configurations for testing the extendded TCAT with varying integrator types, step sizes and initial propellant guesses. The initial propellant was chosen as to be too small and too large, respectively, for half of the configurations. Note that these eight configurations all use a margin of the same size of 0.5 kilograms, which is the standard value for the margin for modeling high-thrust missions. Due to the new convergence algorithm only being used when the propellant mass is insufficient, configurations III, V and VII only make use of the conventional convergence algorithm (Figure 1) while II, IV, VI and VIII only use the new one (Figure 2). The only exception is configuration I where the large inaccuracies can cause the conventional algorithm to dysfunction and therefore the new algorithm is used.

Table 3: Overview of the different configuration settings used to run the ESMO mission (upper) and the SMART-1 mission (lower). Note: C stands for the Cowell integrator and R for Runge-Kutta 8/9.

	I	**II**	**III**	**IV**	**V**	**VI**	**VII**	**VIII**
Integrator type	C	C	R	R	R	R	R	R
Step size [s]	50	50	200	200	200	200	5000	5000
Initial propellant [kg]	40	10	80	30	95	5	80	30
Integrator type	C	C	R	R	R	R	R	R
Step size [s]	200	200	200	200	200	200	5000	5000
Initial ropellant [kg]	165	120	190	125	240	10	240	125

The plots in Figure 6 illustrate the convergence behavior of different configurations tested for ESMO and SMART-1 missions in Table 3. Note that the top row corresponds to the configurations that were run with a Cowell integrator, whereas all of the other rows correspond to results obtained with the RK89 integrator. Note further that the plots in the left column correspond to configurations with an initial propellant mass guess that is higher than the desired value and similarly, the plots within the right column correspond to configurations with initial propellant mass guesses that were lower than the desired value. As for configuration I, Notice that the initial propellant mass for iteration five is higher than the one for iteration four, yet the remaining propellant mass is smaller and even insufficient for iteration five. Similar behavior can be observed for iterations eight, nine and ten, where the remaining propellant mass takes the lowest value in iteration nine, even though the initial propellant mass is successively decreased from iterations eight through ten. This is exactly the type of behavior attributed to the discrepancy between the accuracy of TCAT and of FreeFlyer. Combined with the convergence/iterations section of Table 4, it is apparent in the charts that configurations I and II need more iterations to reach convergence than configurations III to VIII. They also require longer runtime per iteration because their step size is chosen to be much smaller than those of the other configurations.

DOI: 10.13009/EUCASS2022-4800

Moving on to configurations III, V and VII in the left column, a very similar picture is presented across the three plots. Even with that large a step size (VII), the accuracy seems to be more than sufficient and the algorithm still yields the same result for the propellant mass as for the smaller step size, within the expected range of plus or minus the margin. Note, that since the propellant mass was never insufficient during the convergence cycle, only the conventional convergence algorithm was used. Also important to note is that slope mismatching between the remaining propellant (blue) and the initial propellant (red) is never seen here, as opposed to the configurations using the Cowell integrator.

Finally considering configurations IV, VI and VIII in the right column, once again a similar behavior for all of them can be seen. For each of the three configurations, the dashed lines connecting the initial propellant masses start of with a global minimum, then hit a global maximum and finally decrease strictly until convergence occurs. This type of behavior is expected, as the new convergence algorithm takes over as soon as the initial propellant mass is insufficient and then uses a larger m_{sub} given by Equation (3) from the upper boundary. Similar to configurations III and VII, configurations IV and VIII look almost identical and yield the same result for the propellant mass within the expected margin despite the different step sizes. Also, as it is the case for the other configurations that use an RK89 integrator, the slope of the remaining propellant mass always matches the one of the initial propellant mass.

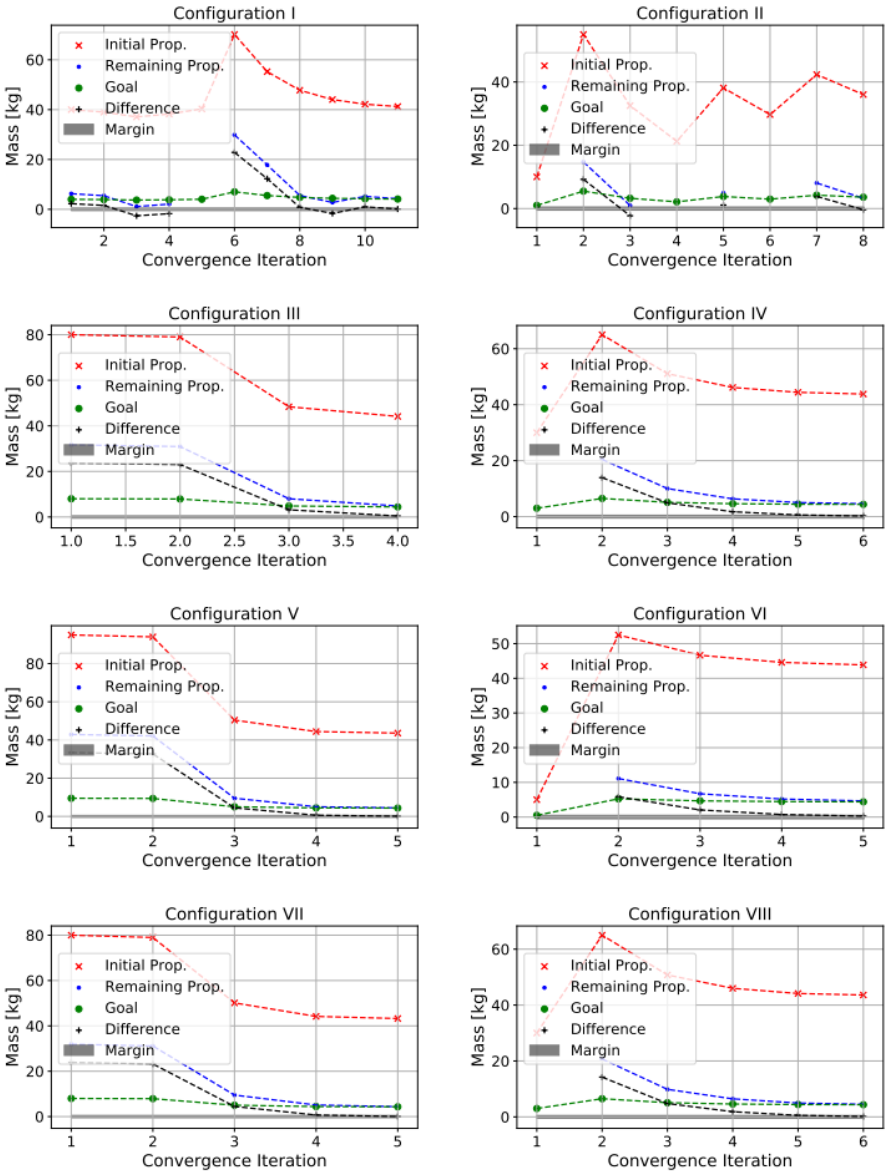

Figure 6: The convergence behavior for the different configurations used to run the ESMO mission.

DOI: 10.13009/EUCASS2022-4800

Table 4: Different configurations and of their corresponding outputs for the ESMO mission.

	I	**II**	**III**	**IV**	**V**	**VI**	**VII**	**VIII**
# iterations (A)	11	8	4	6	5	5	5	6
Runtime (B) [s]	1773	1526	238	171	218	135	58	41
B ÷ A [s]	161	191	60	29	44	27	12	7
Wet mass [kg]	194.8	189.5	180.1	179.8	179.6	179.8	179.2	179.5
Dry mass [kg]	153.5	153.5	135.9	135.9	135.9	135.9	135.9	135.9
Prop mass [kg]	41.2	36.0	44.1	43.8	43.6	43.9	43.2	43.6
Duration [d]	410	400	371	371	371	371	369	370

The convergence behaviors for all the different configurations used to run the SMART-1 mission are illustrated in Figure 7 whose arrangement is identical to Figure 6. Starting again with the top row, it is immediately apparent that configurations I and II required significantly more iterations to reach convergence, as compared to the other configurations. Also, for configuration I, the remaining propellant mass line is not matching the initial propellant mass line in slopes. The effect is especially apparent when considering iterations 17 to 24, where the initial propellant mass remains approximately constant and yet, the remaining propellant mass varies within a range of about 40 kilograms, which is a significant amount of mass compared to the initial propellant mass of around 160 kilograms. This example was mainly included to illustrate the effect of a larger margin on the convergence behavior; convergence is more likely to occur for a larger margin. Other tendencies were similar to those in ESMO except for higher discrepancies. For ESMO, TCAT overestimated the required propellant mass by 73%, while for SMART-1, it overestimated it by 123% as summarized in Table 5. Keep in mind that these values can only be given without uncertainties as of now and their interpretation is thus somewhat difficult. However, efforts should still be made to discuss possible and likely sources of uncertainties and discrepancies, as the knowledge of these will be crucial for the future of TCAT. In this context, it is especially interesting to have a closer look at the ESMO mission, as the lunar transfers in TCAT are modeled very similarly to the models used for ESMO by Colombo et al (2007).

Table 5: Different configurations and of their corresponding outputs for the SMART-1 mission.

	I	**II**	**III**	**IV**	**V**	**VI**	**VII**	**VIII**
# iterations (A)	24	12	4	5	5	6	5	4
Runtime (B) [s]	644	594	82	87	97	84	48	40
B ÷ A [s]	27	50	21	17	19	14	10	10
Wet mass [kg]	445.1	445.6	468.7	469.3	468.6	469.6	469.1	469.7
Dry mass [kg]	286.5	286.5	286.5	286.5	286.5	286.5	286.5	286.5
Prop mass [kg]	158.6	159.1	182.2	182.8	182.1	182.1	182.6	182.2
Duration [d]	245	243	257	258	257	258	258	258

DOI: 10.13009/EUCASS2022-4800

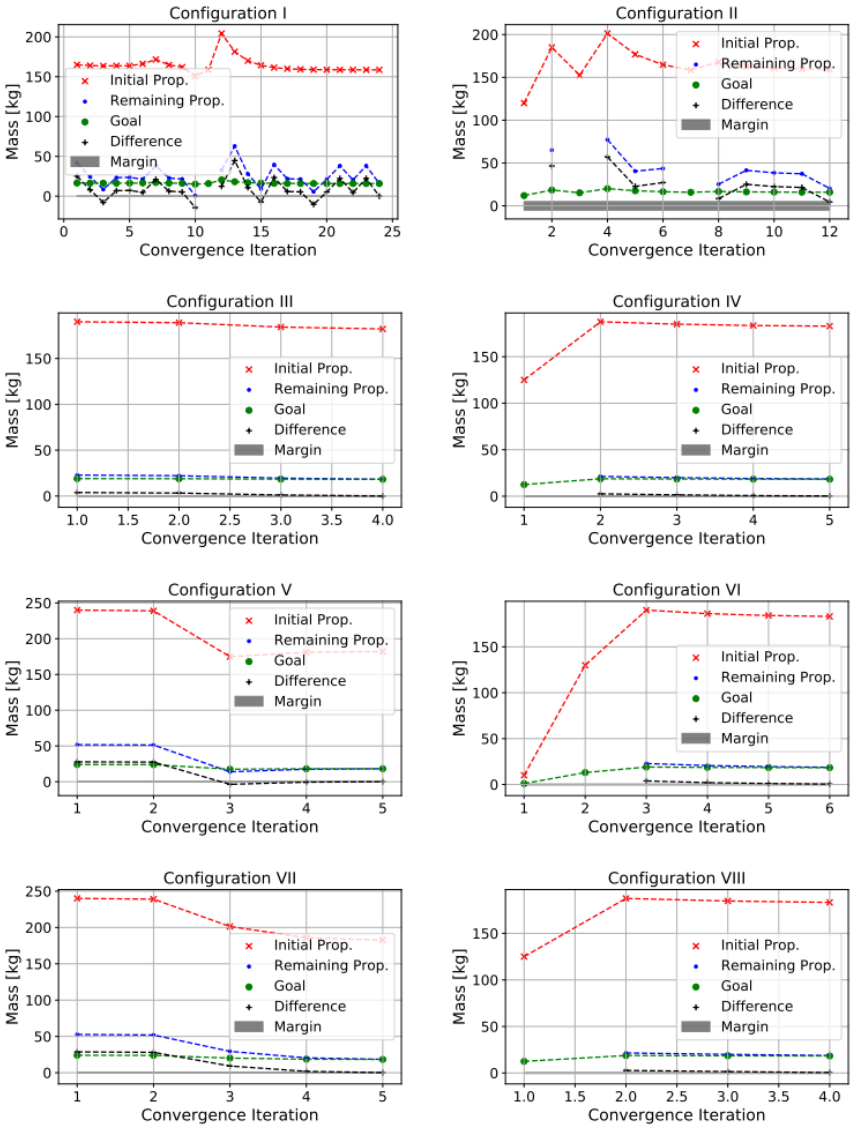

Figure 7: The convergence behavior for the different configurations used to run the SMART-1 mission.

In addition to this, the ESMO mission is also better documented than the SMART-1 mission in terms of propellant masses for the different mission phases. The propellant masses that have been used for the respective mission phases both by the actual ESMO mission and by the one modeled in TCAT (configuration III) are presented in Table 6. Note that due to the different modeling approaches, the actual mission requires some propellant mass (3.9 kg) during lunar capture, while the mission modeled in TCAT does not (0 kg). Very striking in Table 5.1 are the propellant masses for the Earth and the Moon spirals. Apparently, for the Earth spiral, TCAT yielded an identical result, considering the margin of 0.5 kilograms. For the Moon spiral, however, the value computed by TCAT is more than six times as high, or three times as high, when adding the lunar capture propellant mass to the Moon spiral mass for the actual mission. At least for the case of ESMO, the assumption that the initial orbit around Earth is circular does not seem to have a major impact on the result. Another assumption in the model attributable for the mismatch in propellant mass is the final circular orbit around the Moon. The simplifying assumption thereof was to avoid the need for backwards propagation and estimation of the propellant mass in the final lunar orbit. To rule out this assumption as a large contribution to the mismatch, backwards propagation was actually performed for configuration III in a similar manner as done by Colombo et al. (not shown here). The difference in propellant mass was only about 2 kilograms and thus could not account for this large discrepancy.

DOI: 10.13009/EUCASS2022-4800

Table 6: Comparison of the propellant masses for the different mission phases for the ESMO mission as given by Colombo et al. (2007) and as computed by TCAT for configuration III.

	Actual (kg)	**III (kg)**	**Deviation**
Earth spiral	15.9	15.7	-1%
Lunar capture	3.9	0.0	n/a
Moon spiral	3.9	23.6	+505%
Contingency	1.6*	4.8*	+200%
Total	25.3	44.1	+73%

At the moment, the leading hypothesis for the large mismatch is related to the force model that has been used. More specifically, Colombo et al. (2007) use a four-body, unrestricted model to account for the gravitational interactions between the spacecraft and other celestial bodies, meaning they took into account the gravitational attraction of the Moon, the Earth and the Sun. However, TCAT considered only the gravitational attraction of the Moon for the lunar spiral phase. For low lunar orbits, this could be an acceptable assumption, but the initial lunar orbits after lunar capture start at a radius of 60 000 kilometers, which might induce inaccuracies that are greater than expected. Assuming that the Moon, the Earth and the Sun align on the same side of the spacecraft, the lunar gravitation only becomes dominant below a radius of about 30 000 kilometers. Ignoring the gravitational attraction of Earth for the Moon spiral results in a much larger potential difference the spacecraft has to overcome to reach a low lunar orbit and thus to larger fuel consumption. This effect may also explain the slope of Figure 5 (bottom) changing over time. If one were to extrapolate the curve with the initial slope to the end of the plot, i. e. to around 400 days, the final total mass would be around 168 kilograms, instead of around 156 kilograms, thus resulting in five times lower propellant consumption for the Moon spiral. This would correspond to a +20% error in lieu of +505% after 23.6 kilograms is reduced to 4.7 kilograms in Table 6 (comparison with ESMO), which is only slightly higher than the chemical propulsion version of the TCAT. Both the ESMO mission and the SMART-1 mission used elliptical spirals around the Moon, as depicted in Figure 7, whose effect should also be examined in future work [6]. If these phasing effects of elliptical are negligible, errors from the abovementioned line-extrapolation could be tolerated or compensated to provide reasonable fuel economy estimates for space logistics, with improved accuracy or/and versatility compared to Edelbaum's method [7].

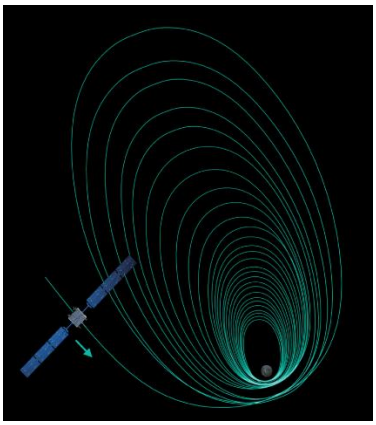

Figure 8: The lunar descent of SMART-1 [6].

3.2 EP Parametrization

Another topic of this paper, albeit very brief, is the survey of specifications for ion engines. The surveyed engines are as follows: NSTAR, Mixi, Scout, SERT-1, Snapshot, Yantar 1/2/3, ATS-4/5/6, Scatha, NEXT, and BHT8000 [8]. Thrust values have been slowly increasing over the course of time in Figure 9 where the outlier on the bottom right corresponds to the Miniature Xenon Ion (Mixi) gridded ion thruster for small satellites. The input power exhibits a

DOI: 10.13009/EUCASS2022-4800

similar trend in Figure 10. Plotting the input power against thrust, the Mixi datapoint is no longer an outlier, implying that a scaling law could be developed for various sizes of propulsion systems. Similar surveys could be done for other subsystems relevant to propulsion, such as propellant tanks or energy storage devices [9, 10].

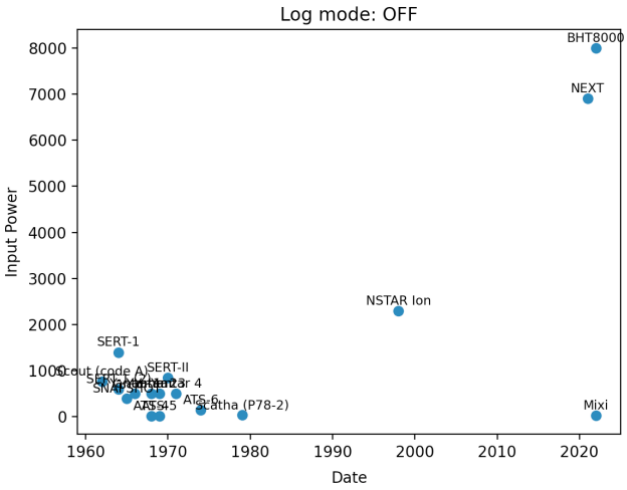

Figure 9: Input power change over time [8].

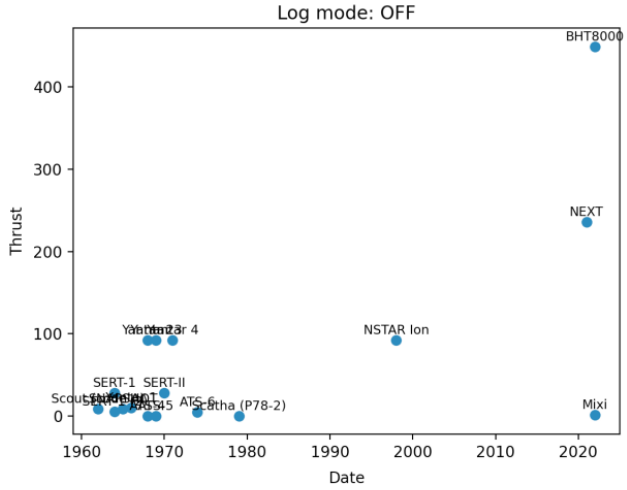

Figure 10: Thrust change over time [8].

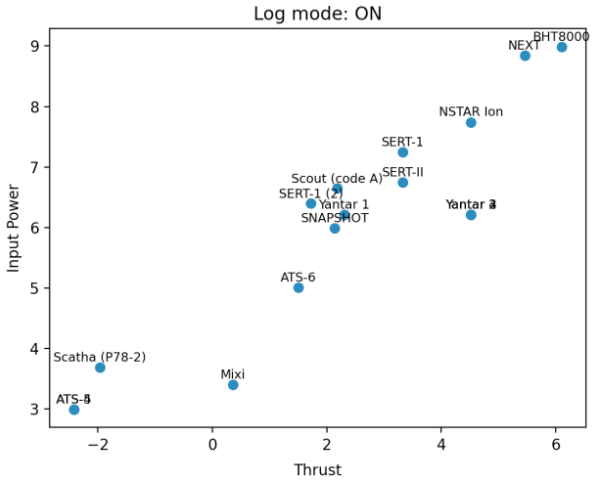

Figure 11: Thrust vs input power [8].

DOI: 10.13009/EUCASS2022-4800

4. Conclusion

The initial question this paper attempted to answer was whether a lightweight/simple tool would be practical to do rapid, accurate spacecraft sizing for electric propulsion in the Earth-Moon system. While this question cannot be clearly answered due to (i) the high deviations of the computed physical output values from the actual values and (ii) the missing information regarding mass breakdowns and uncertainties thereof. However, the findings of this paper suggest that the improvement would not need formidable time given that the major contribution to the deviations in the output values is the force model. It should also be noted that the current implementation is somewhat biased towards the ESMO mission, as it uses a very similar modeling approach. The analysis of the implementation has been limited to ESMO and SMART-1 missions only, but more mission data could be gathered simulate other missions and investigate their results. The database of EP systems and other relevant subsystems could be useful for optimizing the spacecraft size and low-thrust trajectories concurrently as well as expanding the scope of the TCAT beyond the Earth-Moon system [11, 12]. Eventually, the space economy and off-Earth manufacturing aspect might be included in the future TCAT versions [13, 14].

DOI: 10.13009/EUCASS2022-4800

References

[1] Chamot, B., Richard, M., Salmon, T., Pisseloup, A., Cougnet, C., Axthelm, R., Saunders, C., Dupont, C., and Lequette, L., 2013, April. Technology combination analysis tool (TCAT) for Active Debris Removal. In 6th European Conference on Orbital Debris, Darmstadt.

[2] Brancato, G., 2020. Development of a Space Logistics Optimization Tool to Support Decision-Making for Technology Road Mapping. Master's Thesis. École Polytechnique Fédérale de Lausanne.

[3] Huber, P., 2021. Rapid Spacecraft Sizing & Logistics Tool: Extension to Electric Propulsion. Master's Thesis. Eidgenössische Technische Hochschule Zürich.

[4] Bounova, G.A., Ahn, J., Hofstetter, W., Wooster, P., Hassan, R., and De Weck, O.L. Selection and technology evaluation of Moon/Mars transportation architectures. Collection of Technical Papers - AIAA Space 2005 Conference and Exposition, 3:1421–1430, 2005. doi: 10.2514/6.2005-6790.

[5] Colombo, C., Novak, D., and Heiligers, J. Low-thrust trajectories design for the European Student Moon Orbiter Mission. International Astronautical Federation - 58th International Astronautical Congress 2007, 12:7975–7988.

[6] Wikipedia, SMART-1, 2022. Available online: https://en.wikipedia.org/wiki/SMART-1 (accessed on 1 July 2022).

[7] Edelbaum, T.N. 1961. Propulsion requirements for controllable satellites. *ARS Journal*, 31(8):1079–1089, doi: 10.2514/8.5723.

[8] Cristofoletti, R. 2022. Parametric study of spacecraft electric propulsion systems, Bachelor's Thesis.

[9] Paek, S. W., Balasubramanian, S., Kim, S., and de Weck, O. 2020. Small-satellite synthetic aperture radar for continuous global biospheric monitoring: A review. *Remote Sensing*, 12(16), 2546.

[10] Paek, S. W., Kim, S., and de Weck, O. 2019. Optimization of reconfigurable satellite constellations using simulated annealing and genetic algorithm. *Sensors*, 19(4), 765.

[11] Paek, S. W. 2017. Concurrent design optimization of Earth observation satellites and reconfigurable constellations. Journal of the British Interplanetary Society, 70, 19-35.

[12] Paek, S. W., de Weck, O., Hoffman, J., Binzel, R., and Miller, D. 2020. Optimization and decision-making framework for multi-staged asteroid deflection campaigns under epistemic uncertainties. *Acta Astronautica*, 167, 23-41.

[13] Chavy-Macdonald, M.A., Oizumi, K., Kneib, J.P. and Aoyama, K., 2021. The cis-lunar ecosystem—A systems model and scenarios of the resource industry and its impact. *Acta Astronautica*, 188, pp.545-558.

[14] Paek, S. W., Balasubramanian, S., and Stupples, D. 2022. Composites Additive Manufacturing for Space Applications: A Review, *Materials*, In print.